ELSEVIER

Advances in Engineering Software 31 (2000) 339–346

ADVANCES IN ENGINEERING SOFTWARE

www.elsevier.com/locate/advengsoft

Smoothed surface gradients for panel methods

J. D'Elía*, M. Storti, S. Idelsohn

Centro Internacional de Métodos Computacionales en Ingeniería (CIMEC) INTEC (UNL-CONICET), Güemes 3450, 3000-Santa Fe, Argentina

Accepted 18 November 1999

Abstract

A weak form to compute the dipolar and monopolar surface gradients, related to a low-order panel method, is shown. The flow problem is formulated by means of a three-dimensional potential model and the discretization is based on Morino's formulation for the perturbation velocity potential. On the body surface, this representation reduces to a boundary integral equation with the source (or monopolar) and the doublet (or dipolar) densities. The first of the two is found by application of the boundary flow condition, and the second one is the unknown over the body surface. A lower panel method is used for the analytic integrations of both the monopolar and dipolar influence coefficients. The surface velocity field is computed after solving the linear system, with a strong and a weak form of the Stokes theorem, which is oriented to fairly non-structured panel meshes. The proposed method is validated by comparing the numerical results with analytical ones for an isolated sphere and includes a prediction over a car-like configuration.

Keywords: Potential flows; Surface velocities; Boundary elements

1. Introduction

Panel methods are widely accepted in the aerospace and naval industry for calculating potential flows [1,2]. In some problems, a two-dimensional (2D) approach is sufficient, for instance, flows past multicomponent airfoils, infinite cascade, ground effects and wind tunnels [3,4] while in other cases a three-dimensional (3D) approach is necessary. The 3D flows problem in these areas have special features that distinguish from other types [5]. In the first place, the body shapes are often quite complicated and, then, the methods applicable only to smooth shapes are neither fully useful nor are those whose computing costs increase rapidly with the boundary complexity. Also, the flow magnitudes are often very sensitive to small details of the body shape and the difference between good and bad aero/hydro dynamic surfaces can be quite subtle; therefore a useful method must be able to discriminate between rather similar shapes. Often, it is desired to know not only the solution on the boundary but also its surface gradient. The most widely used approach to its computation in panel methods, is based on the use of the integral representation related with the formulation employed, but for the Morino's formulation [6] a rather simpler device was proposed by Maître [7]. In particular, this author had shown that a numerical scheme for the doublet surface gradient based on a special form of the Stokes theorem [8], is not well suited since its computational performance is too degraded with fairly non-structured panel meshes. In order to overcome this shortcoming, we propose in this work an alternative way using a weak form of the Stokes theorem. This weak form allows us to compute smoothed surface gradient fields, for both doublet and source layers (or dipolar and monopolar ones, respectively) which are employed in Morino's formulation and is oriented to fairly non-structured panel meshes.

2. Potential formulation review

Consider an exterior flow problem, see Fig. 1, where Ω is the exterior region to the wetted surface Γ_S of a stream-like body. The x-axis is parallel to the non-perturbed velocity $\mathbf{u}_\infty$, the z-axis positive upwards and the y-axis results in a right-turn sequence (x,y,z). The potential velocity field is given by $\mathbf{u} = \nabla\Phi$, where Φ is the total velocity potential, which satisfies the Laplace equation in the flow region Ω and it is split as $\Phi = \mathbf{u}_\infty^{\mathrm{T}}\mathbf{x} + \phi$, where $\mathbf{x} = (x, y, z)$ is the position vector and ϕ is the perturbation velocity potential. The kinematic boundary conditions are the slip condition $\partial_n\Phi = 0$ at the wetted body surface while, at the infinity, the perturbation velocity potential tends to zero for external

* Corresponding author. Tel.: + 54-342-4559175; fax: + 54-342-4550944.

E-mail address: rngtm@arcride.edu.ar (J. D'Elía).

0965-9978/00/$ - see front matter
PII: S0965-9978(99)00059-9

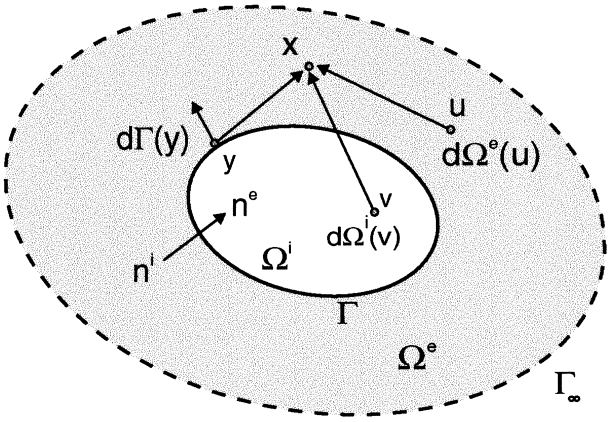

Fig. 1. Geometry for exterior flow problems.

flows, i.e. $\phi(\mathbf{x}) \to 0$ for $|\mathbf{x}| \to \infty$. Then, the governing equations for the solution Φ of this potential flow model are:

$$\begin{cases} \Delta\Phi = 0 & \text{in } \Omega; \\ \partial_n \Phi = 0 & \text{at } \Gamma_S; \\ \Phi \to \mathbf{u}_\infty^T \mathbf{x} & \text{for } |\mathbf{x}| \to \infty. \end{cases} \tag{1}$$

3. Panel formulation

The Morino integral formulation can be written as

$$\frac{1}{2}\mu(\mathbf{x}) + \frac{1}{4\pi}\int_\Gamma \mathrm{d}\Gamma_\mathbf{y} \frac{\partial}{\partial n}\frac{1}{r}\mu(\mathbf{y}) = \frac{1}{4\pi}\int_\Gamma \mathrm{d}\Gamma_\mathbf{y}\frac{1}{r}\sigma(\mathbf{y}) \tag{2}$$

for $\mathbf{x}$ over Γ;

with

$$\sigma = (-\mathbf{u}_\infty, \mathbf{n}) \tag{3}$$

where μ and σ are the double and single layer densities over the surface Γ, $r = |\mathbf{x} - \mathbf{y}|$ is the Euclidean distance between the field point $\mathbf{x}$ and the source point $\mathbf{y}$, and $\mathbf{n}$ is the (exterior) unit normal. We discretize it using a low-order panel method. The mesh employs a low-order representation of the body surface by means of a polyhedral with n flat surfaces over the wetted body surface. We impose the discretized boundary integral equation by collocation at the centroids of the panels, to set up the discrete lineal system $\mathbf{A}\boldsymbol{\mu} = \mathbf{b}$, where $\mathbf{A}$ is the (bipolar) matrix system and $\boldsymbol{\mu}$ is the bipolar vector evaluated at the centroids of the n-panels, i.e. $\boldsymbol{\mu} = [\mu(\mathbf{x}_1)\ldots\mu(\mathbf{x}_n)]^T$, and $\mathbf{b}$ is the source vector. The source vector $\mathbf{b} = \mathbf{C}\boldsymbol{\sigma}$, is the product of the monopolar influence matrix $\mathbf{C}$ and the flow vector $\boldsymbol{\sigma} = [\sigma(\mathbf{x}_1)\ldots\sigma(\mathbf{x}_n)]^T$, obtained by means of the *slip* boundary condition on the solid walls, that is, $\sigma_j = -\mathbf{u}_{\infty,j}^T\mathbf{n}_j$, where $\mathbf{n}_j$ is the panel normally oriented to the wetted side. The bipolar and monopolar influence matrices A_{ij}, C_{ij} are given by the surface integrals

$$A_{ij} = \frac{1}{4\pi}\int_\Gamma \mathrm{d}\Gamma_j \frac{\mathbf{r}_{ij}^T\mathbf{n}_j}{r_{ij}^3} \text{ and } C_{ij} = \frac{1}{4\pi}\int_\Gamma \mathrm{d}\Gamma_j \frac{1}{|\mathbf{r}_{ij}|} \tag{4}$$

for $i, j = 1, 2, \ldots, n$;

where $\mathbf{r}_{ij} = |\mathbf{x}_i - \mathbf{x}_j|$ is the Euclidean distance between the centroid $\mathbf{x}_i$ and the integration point $\mathbf{x}_j$ over the j-panel surface with $\mathbf{x} = (x, y, z)$. These integrals can be evaluated in a closed form following an analogous procedure proposed by Medina and Liggett [9], e.g. see also D'Elía [13,14]. Both influence matrices $\mathbf{A}$ and $\mathbf{C}$ are dense and non-symmetric and its vectorial computation can be obtained as follows: on each j-panel, both double and single unitary density layers are imposed. Then, it is computed with the fields measured over all centroids $\mathbf{x}_i$, obtaining the bipolar and the monopolar influence column vectors $\mathbf{a}_j, \mathbf{c}_j$. Both column vectors are simultaneously computed since they have several transcendent expressions which are similar and, then, it is evaluated the as discrete operators $\mathbf{A} = [\mathbf{a}_1\ldots\mathbf{a}_n]$ and $\mathbf{C} = [\mathbf{c}_1\ldots\mathbf{c}_n]$.

4. Surface velocity computation

The velocity field $\mathbf{u}$ on the body surface Γ, is obtained by means of

$$\mathbf{u} = \mathbf{u}_\infty + \mathbf{u}' + \mathbf{u}'' \qquad \text{at } \Gamma; \tag{5}$$

where $\mathbf{u}'$ and $\mathbf{u}''$ are the monopolar and dipolar velocities, respectively. They are found from (e.g. see Ref. [7])

$$\begin{cases} \mathbf{u}' = \sigma\mathbf{n}; \\ \mathbf{u}'' = -\nabla\mu; \end{cases} \tag{6}$$

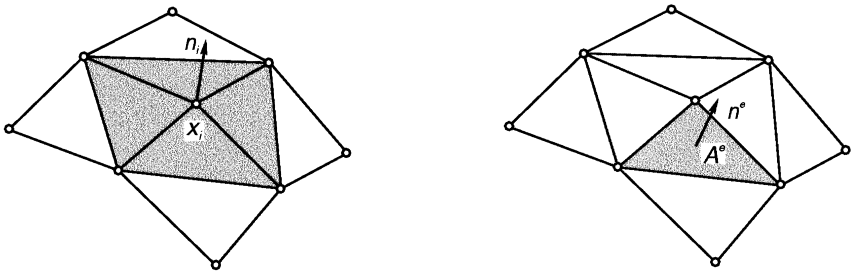

Fig. 2. A_i-panel patch around the i-node.

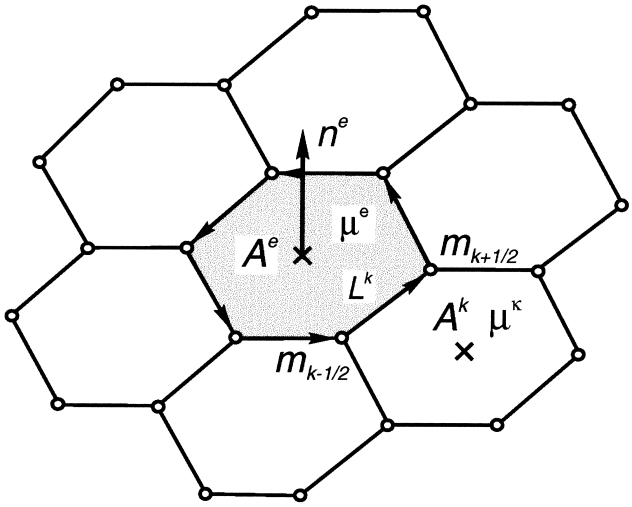

Fig. 3. Panel dipolar gradient by means of the Stokes theorem.

where ∇ is the surface gradient and $\mathbf{n}$ is the unit normal to the surface. The dipolar layer μ is found solving the boundary integral Eq. (2), and the monopolar layer σ is from the slip boundary Eq. (3). In a low order panel method, both of them are piecewise-constant on the panel mesh. A nodal velocity computation can be obtained averaging over the A_i-panel *patch* adjacent to the *i*-node, as is shown in Fig. 2. We show a strong (classical) form and a weak one for the perturbation velocities $\mathbf{u}'$ and $\mathbf{u}''$, where the weak form considered in this work is developed only for triangular panels.

4.1. Strong form for the perturbation velocities

A simple average of both velocities $\mathbf{u}'_i$ and $\mathbf{u}''_i$ can be obtained by using a surface average over the A_i-panel patch around the *i*-node. For the monopolar one, we write

$$\mathbf{u}'_i = \frac{1}{A}\sum_{e=1}^{n_p} \mathbf{u}_\sigma^e A^e; \tag{7}$$

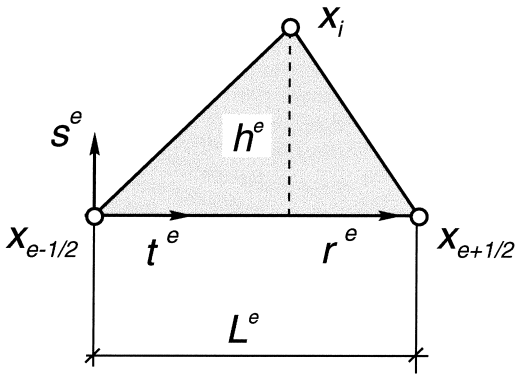

Fig. 4. Geometrical description for the shape function N_i^e over a triangle panel.

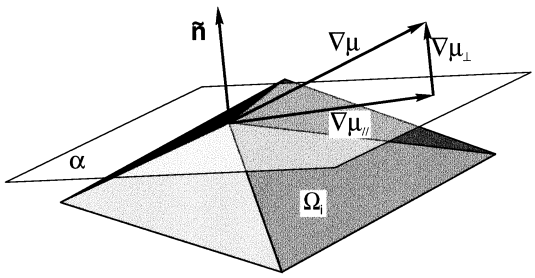

Fig. 5. Spurious component $\nabla\mu_\perp$ in the weak dipolar gradient.

with

$$A = \sum_{e=1}^{n_p} A^e; \tag{8}$$

where A^e is the panel area, n_p is the number of panels on the A_i-panel patch and

$$\mathbf{u}_\sigma^e = \sigma^e \mathbf{n}^e; \tag{9}$$

is the monopolar velocity on the *e*-panel, being $\sigma^e = (-\mathbf{u}_\infty, \mathbf{n}^e)$ and $\mathbf{n}^e$ the surface density and the (constant) unit normal, respectively. In the same manner, we have for the dipolar velocity

$$\mathbf{u}''_i = \frac{1}{A}\sum_{e=1}^{n_p} \mathbf{u}_\mu^e A^e; \tag{10}$$

where

$$\mathbf{u}_\mu^e = -\nabla\mu^e; \tag{11}$$

is the average dipolar velocity over the *e*-panel (constant) and ∇ is the surface gradient. For its computation, we employ the vectorial form of the Stokes theorem (e.g. see Refs. [7,8])

$$\int_{A^e} (\mathbf{n}^e \times \nabla\mu^e)\, \mathrm{d}A = \int_{L^e} \mu^e\, \mathrm{d}\mathbf{L}; \tag{12}$$

where L^e is the contour of the panel surface A^e and $\mathbf{n}^e$ is its unit normal. When both the dipolar gradient $\nabla\mu^e$ and the unit normal $\mathbf{n}^e$ are constant over the panel surface A^e, this

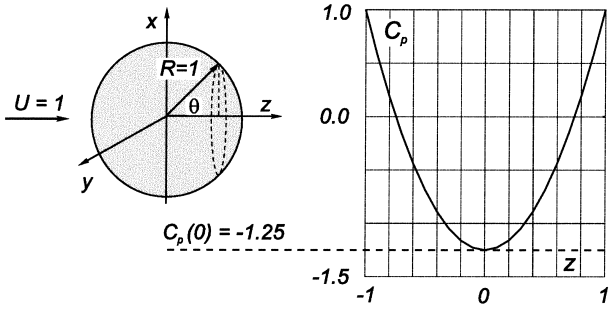

Fig. 6. Potential flow around a sphere (left), and analytical pressure coefficient (right).

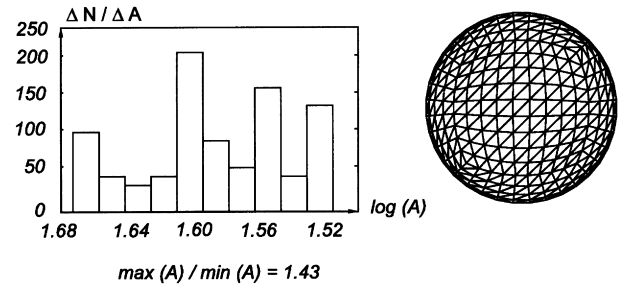

Fig. 7. Sphere with a structured mesh (right), and panel area histogram (left).

reduces to evaluate

$$\nabla\mu^e = -\frac{\mathbf{n}^e}{A^e} \times \int_{L^e} \mu^e \, \mathrm{d}\mathbf{L}; \tag{13}$$

which can be discretized, over an e-panel of n_s sides, see Fig. 3, as

$$\nabla\mu^e = -\frac{\mathbf{n}^e}{A^e} \times \sum_{k=1}^{n_s} \tilde{\mu}^k \mathbf{L}^k; \tag{14}$$

where $\mathbf{L}^k$ is its k-side and $\tilde{\mu}^k$ is some average value, for instance, we have taken

$$\tilde{\mu}^k = \begin{cases} (\mu^e + \mu^k)/2 & \text{arithmetic average;} \\ (\mu^e A^e + \mu^k A^k)/(A^e + A^k) & \text{surface average.} \end{cases} \tag{15}$$

4.2. Weak form for the perturbation velocities

In order to develop a weak form of the average velocities $\mathbf{u}'_i$ and $\mathbf{u}''_i$, we consider only triangular panels and introduce the nodal shape function for the i-node (in the FEM sense)

$$N_i = \sum_{e=1}^{n_p} N_i^e; \tag{16}$$

where N_i^e is the elemental shape function of the e-triangular panel on the A_i panel patch. This function is chosen in such a way that

$$N_i^e(\mathbf{x}) = \begin{cases} 1 & \text{for } \mathbf{x} = \mathbf{x}_i; \\ 0 & \text{for } \mathbf{x} = \mathbf{x}_{e-1/2} + \mathbf{t}^e\lambda; \end{cases} \tag{17}$$

where λ is a free parameter and

$$\mathbf{t}^e = \frac{\mathbf{r}^e}{|\mathbf{r}^e|}; \tag{18}$$

is the unit tangent vector along the e-side opposite to the i-node and

$$\mathbf{r}^e = \mathbf{x}_{e+1/2} - \mathbf{x}_{e-1/2}; \tag{19}$$

is the edge vector, where $\mathbf{x}_{e+1/2}$ and $\mathbf{x}_{e-1/2}$ are its vertices of the e-side opposite to the i-node. That is, the chosen shape elemental function N_i^e has a unit value on the i-node, null over the opposite side and a linear dependence in the interval between them and, then, its gradient over the e-panel is constant and equals to

$$\nabla N_i^e = \frac{1}{h^e}\mathbf{s}^e; \tag{20}$$

where h^e is the panel height, $\mathbf{s}^e$ is the unit vector obtained as

$$\mathbf{s}^e = \mathbf{n}^e \times \mathbf{t}^e; \tag{21}$$

defining the unit vectors $(\mathbf{t}^e, \mathbf{s}^e, \mathbf{n}^e)$, a local coordinate system at the e-edge, see Fig. 4. Now, the panel area can be computed as $A^e = h^e L^e/2$, where $L^e = |\mathbf{r}^e|$ is the opposite side length of the i-node and from this

$$h^e = \frac{2A^e}{L^e}. \tag{22}$$

Introducing Eqs. (21) and (22) into Eq. (20), we obtain

$$\nabla N_i^e = \frac{L^e}{2A^e}(\mathbf{n}^e \times \mathbf{t}^e) = \frac{\mathbf{n}^e \times \mathbf{r}^e}{2A^e}; \tag{23}$$

where also $\mathbf{r}^e = L^e\mathbf{t}^e$. A weak dipolar gradient can be obtained with the nodal shape function N_i and the standard Galerkin procedures [10]. Let us consider the weighted

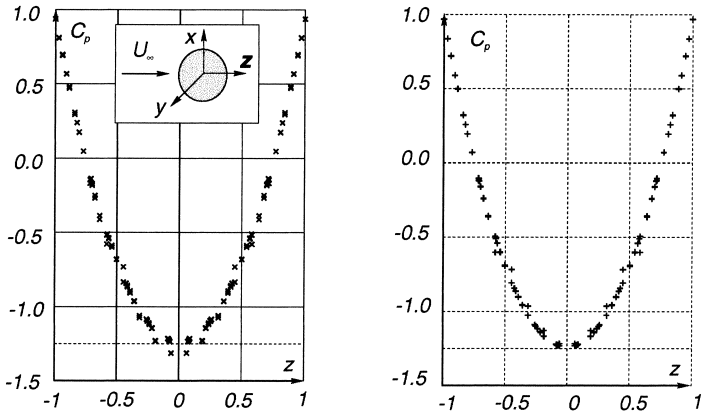

Fig. 8. Pressure coefficient $C_p(z)$ for a structured panel mesh over a sphere using a strong form (left) and a weak one (right), respectively.

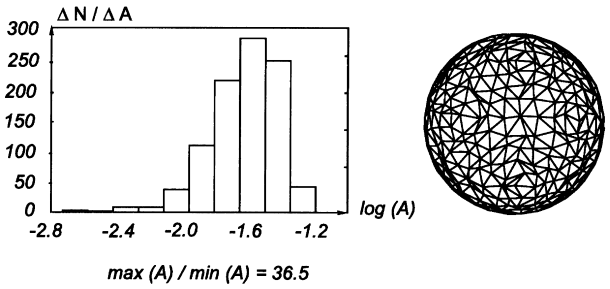

Fig. 9. Panel perturbed mesh over a sphere (right), and panel area histogram (left).

average over the A_i-panel patch

$$\tilde{\nabla}\mu_i = \frac{\gamma_i}{M_i}; \tag{24}$$

where

$$M_i = \sum_{e=1}^{n_s} M_i^e; \tag{25}$$

$$M_i^e = \int_{A_i} N_i \nabla\mu \, \mathrm{d}A; \tag{26}$$

$$\gamma_i = \sum_{e=1}^{n_s} \gamma_i^e; \tag{27}$$

$$\gamma_i^e = \int_{A^e} N_i^e \nabla\mu^e \, \mathrm{d}A; \tag{28}$$

Integration by parts, the right-hand side of Eq. (28) results in

$$\int_{A^e} N_i^e \nabla\mu^e \, \mathrm{d}A = -\int_{A^e} \mu^e \nabla N_i^e \, \mathrm{d}A; \tag{29}$$

It is well known in the finite element context [11], the following identity

$$\int_{A^e} N_i^e \, \mathrm{d}A = \frac{A^e}{3}; \tag{30}$$

where N_i is linear and A^e is a triangular element. Therefore,

$$\sum_{e=1}^{n_p} \int_{A^e} N_i^e \, \mathrm{d}A = \frac{1}{3} \sum_{e=1}^{n_p} A^e; \tag{31}$$

that is

$$M_i = \frac{A_i}{3}; \tag{32}$$

introducing Eqs. (23) and (32) into Eq. (24), we arrive to the weak dipolar gradient

$$\tilde{\nabla}\mu_i = \frac{-3}{2A_i} \sum_{e=1}^{n_s} \mu^e (\mathbf{n}^e \times \mathbf{r}^e). \tag{33}$$

4.3. Spurious weak component

In general, the weak dipolar gradient $\tilde{\nabla}\mu_i$ obtained with Eq. (33), besides a tangential component $\tilde{\nabla}_{\parallel}\mu_i$ on the discrete tangent plane at the node, contains a *spurious* component $\tilde{\nabla}_{\perp}\mu_i$ perpendicular to the tangent plane, see Fig. 5, that is,

$$\tilde{\nabla}\mu_i = \tilde{\nabla}_{\parallel}\mu_i + \tilde{\nabla}_{\perp}\mu_i. \tag{34}$$

As only the tangential component $\tilde{\nabla}_{\parallel}\mu_i$ has physical sense, then we must eliminate the spurious one $\tilde{\nabla}_{\perp}\mu_i$. We note that the spurious component is also present when we impose a unitary dipolar density over the A_i-panel patch and, then, assuming a linear relation between both cases, we write

$$\begin{cases} \tilde{\nabla}_{\perp}\mu_i = \alpha_i \tilde{\nabla}\mu_i^1; \\ \tilde{\nabla}_{\parallel}\mu_i = \tilde{\nabla}\mu_i - \alpha_i \tilde{\nabla}\mu_i^1; \end{cases} \tag{35}$$

where α_i is a nodal proportionality factor, and $\tilde{\nabla}\mu_i^1$ is the unitary dipolar gradient obtained by means of Eq. (33), when $\mu_i = 1$ is imposed on the A_i-panel patch, resulting in

$$\tilde{\nabla}\mu_i^1 = \frac{-3}{2A_i} \sum_{e=1}^{n_s} (\mathbf{n}^e \times \mathbf{r}^e); \tag{36}$$

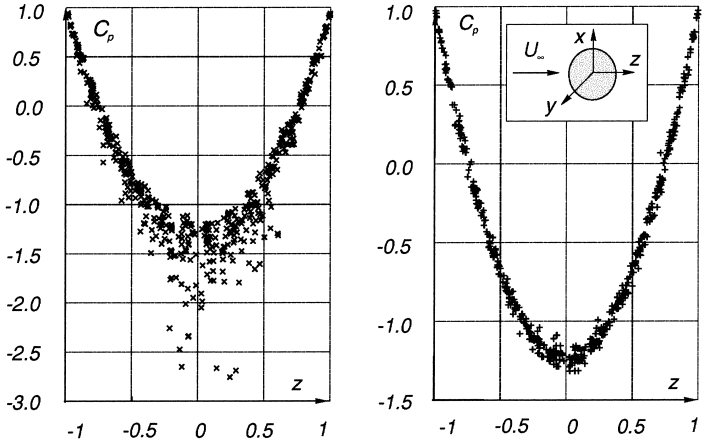

Fig. 10. Pressure coefficient $C_p(z)$ for a non-structured panel mesh over a sphere using a strong form (left) and a weak one (right), respectively.

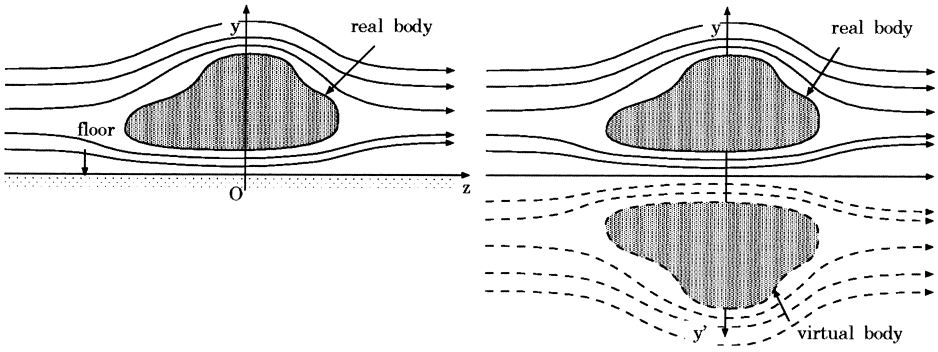

Fig. 11. Sketch for the attached potential flow around a car-like body with the floor's influence.

which is orthogonal to the tangential one

$$(\tilde{\nabla}\mu_i^1, \tilde{\nabla}_{\parallel}\mu_i) = 0. \tag{37}$$

Replacing Eq. (35) into Eq. (37) we find

$$\alpha_i = \frac{(\tilde{\nabla}\mu_i, \tilde{\nabla}\mu_i^1)}{(\tilde{\nabla}\mu_i^1, \tilde{\nabla}\mu_i^1)} \tag{38}$$

which is valid, if and only if

$$|\tilde{\nabla}\mu_i^1| \neq 0. \tag{39}$$

The singular case $|\tilde{\nabla}\mu_i^1| = 0$ occurs, for instance, when the A_i-panel patch is flat, as all unit normals $\mathbf{n}^e$ are equal to $\mathbf{n}$,

$$\tilde{\nabla}\mu_i^1 = \frac{-3}{2A_i}\mathbf{n} \times \sum_{e=1}^{n_s} \mathbf{r}^e; \tag{40}$$

whereas

$$\sum_{e=1}^{n_s} \mathbf{r}^e = \mathbf{0}; \tag{41}$$

since it is a vectorial closed sum. Nevertheless, in this case, Eq. (33) can be used for plane patches. A further useful consequence of the procedure proposed to eliminate the spurious component, is the weak normal unit vector

$$\tilde{\mathbf{n}}_i = \frac{\tilde{\nabla}\mu_i^1}{|\tilde{\nabla}\mu_i^1|}. \tag{42}$$

In brief, the weak monopolar and dipolar velocities are found from

$$\begin{cases} \tilde{\mathbf{u}}'_i = \sigma_i \tilde{\mathbf{n}}_i; \\ \tilde{\mathbf{u}}''_i = -\tilde{\nabla}_{\parallel}\mu_i; \end{cases} \tag{43}$$

if the condition (39) is fully verified.

5. Numerical examples

5.1. A sphere

In order to show the suitability of the proposed method, we have considered the flow around a sphere of radius $R = 1$ with non-perturbed speed $U = 1$. The analytical solution for the surface velocity $u(\theta)$ is [12]

$$u(\theta) = (3/2)U \sin(\theta); \tag{44}$$

and the pressure coefficient $C_p(\theta)$ is found from

$$C_p(\theta) = 1 - \frac{u(\theta)^2}{U^2}; \tag{45}$$

we have, see Fig. 6,

$$C_p(\theta) = 1 - \tfrac{9}{4}\sin^2(\theta); \tag{46}$$

where $\theta = \arccos(z/R)$. For the numerical solution, we have considered two meshes both with 1000 triangular panels. The first one is shown in Fig. 7 and is nearly structured. In Fig. 8, we show the pressure coefficient $C_p(\theta)$ z-axis obtained with the weak and strong formulations. In the last case, we can see a small tendency toward dispersion. The second mesh is shown in Fig. 9 and is non-structured. It is obtained from the first one with a small noise $\epsilon\mathbf{x} = O(h)$

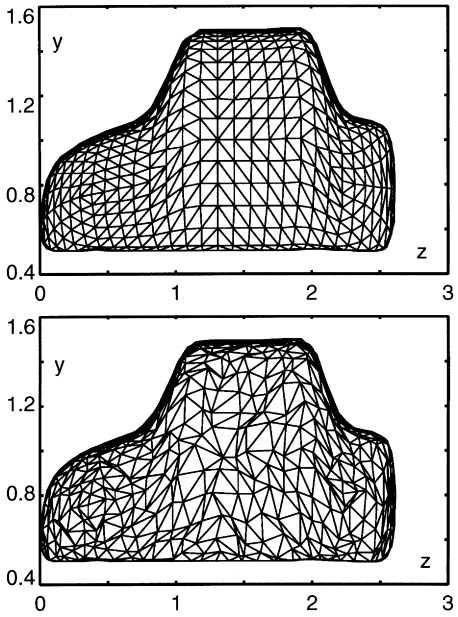

Fig. 12. Car-like meshes with 3100 panels: a structured mesh (left) and a non-structured one (right).

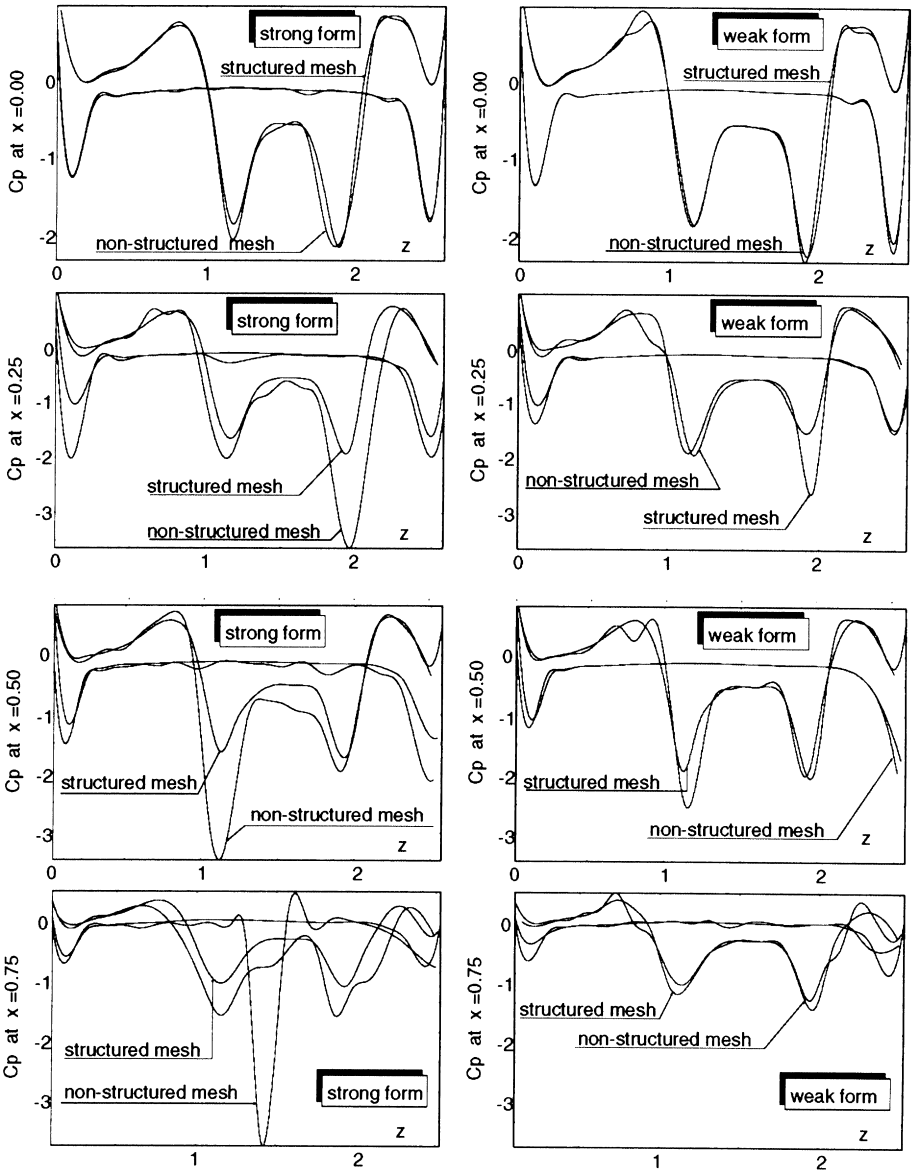

Fig. 13. Pressure coefficient $C_p(z)$ over a car-like body, on section cuts at $x/B = 0,\ 1/4,\ 1/2,\ 3/4$, for structured and non-structured meshes of 3100 panels, as a strong form (left) and a weak one (right).

added to the nodal coordinates, where h is an average diameter of the panels, then we have re-projected to the unit sphere, verifying that the panels do not degenerate. In Fig. 10, we show the pressure coefficient $C_p(\theta)$ along the z-axis obtained with both formulations, where the dispersion tendency of the strong form is evident while the weak form is clearly more robust.

5.2. Car-like configuration

We have considered the non-separated potential flow around a 3D car-like body with the floor influence, as sketched in Fig. 11. As a first approach, the floor influence could be taken into account with a panel mesh over a large but finite floor panel mesh, but this strategy introduces an error due to the plane boundary effects and also the computational cost will be expensive as larger planes are considered. In order to overcome this short-coming, we observe that the flow regime is equivalent to consider a mirrored configuration with respect to the floor (real body + image). In such a case, we have a symmetric virtual car-like body and it is not necessary to introduce the plane. We, then, have a total number of panels, which is twice the number of panels on the body. But, due to the symmetry of the flow, the unknown potentials on the image can be eliminated in terms of the potentials on the body, and the resulting CPU time is almost the same as for the isolated body. We performed numerical experiments with a (smooth) structured mesh and a non-smooth topologically structured one (in brief: structured and non-structured meshes,

respectively). The panel mesh, for each mesh type, has 3100 triangular panels, see Fig. 12. The symmetry of the velocity potential with respect to the floor also allows us to reduce the effective dimension of the linear system. The pressure coefficients $C_p(z)$ are shown in Fig. 13, on section cuts, at $x/B = 0$, 1/4, 1/2, 3/4, the strong form (left-hand side) is much more sensitive than the weak one (right-hand side).

6. Conclusions

We have considered a weak form for the computation of the dipolar and monopolar surface gradients related to a low-order panel method. The flow problem was formulated by means of a 3D potential model and the method of discretization was based on Morino's formulation for the perturbation velocity potential. On the body surface this representation was reduced to an integral equation with source and the doublet densities. The first one was found by application of the boundary condition, and the second one is the unknown over the surface of the body. A low-order panel method was used for the analytic integrations of the monopolar and dipolar influence coefficients. Then, a weak form of the Stokes theorem was developed for the surface gradient computation, which was oriented to fairly non-structured panel meshes. This weak form allows us to overcome the poor performance of the standard one in this kind of meshes. The overall approach is limited by the restrictions of the potential flow model and the weak surface gradient computation is restricted to triangular flat panels. Future work will be focused on the extension of weak forms to panels with an arbitrary number of sides or to high-order panel formulations.

Acknowledgements

This work has received financial support from Consejo Nacional de Investigaciones Científicas y Técnicas (CONICET, Argentina) and Banco Interamericano de Desarrollo (BID) through grant BID 802/OC-AR PID Nr. 26, and from Universidad Nacional del Litoral (Argentina). We made extensive use of Free Software Foundation/GNU-Project resources.

References

[1] Morino L, Kuo CC. Subsonic potential aerodynamics for complex configurations: a general theory. AIAA Journal 1974;12:191–7.
[2] Katz J, Plotkin A. Low-speed aerodynamics, from wing theory to panel methods. New York: McGraw-Hill, 1991.
[3] Mokry M. Complex variable boundary element method for external potential flows, 28th Aerospace Sciences Meeting, January 8–11, Reno, NV, 1990.
[4] Storti M, D'Elía J, Idelsohn S. CVBEM formulation for multiple profiles and cascades. App Mech Rev Part 2 1995;48(11):203–10.
[5] Hess JL. Review of the historical development of surface source methods. In: Morino L, editor. Computational methods in potential aerodynamics, Berlin: Springer, 1985.
[6] Morino L, editor. Computational methods in potential aerodynamics Berlin: Springer, 1985.
[7] Maître T. Modelisation de l'ecoulémént autour d'une hélice marine par la méthode du potentiel. Tesis Doctoral, Institut National Polytechnique de Grenoble, 1988.
[8] Smirnov H. A course of high mathematics (t. 4: Integral equations and partial differential equations). London: Pergamon Press, 1964.
[9] Medina DE, Liggett JA. Three-dimensional boundary element computation of potential flow in fractured rock. Int J Num Meth Engng 1988;26:2319–30.
[10] Zienkiewicz OC, Taylor RL. Finite element method. 4th ed.. New York: McGraw-Hill, 1989.
[11] Segerlind L. Applied finite element analysis. New York: Wiley, 1983.
[12] Streeter VL, editor. Handbook of fluid dynamics New York: McGraw-Hill, 1961.
[13] D'Elía J, Storti M, Idelsohn S. A closed form for low-order panel methods. Advances in Engineering Software 2000;31:347–53.
[14] D'Elía J, Storti M, Idelsohn S. Iterative solution of panel discretizations for potential flows. The modal/multipolar preconditioning. Int J Num Meth Fluids 2000;32:1–2.